Hu, C., & Rarity, J. (2015). Extended linear regime of cavity-QED enhanced optical circular birefringence induced by a charged quantum dot. PHYSICAL REVIEW B, 91(7), 1 - 12. [075304]. 10.1103/PhysRevB.91.075304

Extended linear regime of cavity-QED enhanced optical circular birefringence induced by a charged quantum dot

C. Y. Hu* and J. G. Rarity†

Department of Electrical and Electronic Engineering, University of Bristol, University Walk, Bristol BS8 1TR, United Kingdom

(Received 12 September 2014; revised manuscript received 23 January 2015; published 10 February 2015)

Giant optical Faraday rotation (GFR) and giant optical circular birefringence (GCB) induced by a single quantum-dot spin in an optical microcavity can be regarded as linear effects in the weak-excitation approximation if the input field lies in the low-power limit [Hu *et al.*, Phys. Rev. B **78**, 085307 (2008); **80**, 205326 (2009)]. In this work, we investigate the transition from the weak-excitation approximation moving into the saturation regime comparing a semiclassical approximation with the numerical results from a quantum optics toolbox [Tan, J. Opt. B **1**, 424 (1999)]. We find that the GFR and GCB around the cavity resonance in the strong-coupling regime are input field independent at intermediate powers and can be well described by the semiclassical approximation. Those associated with the dressed state resonances in the strong-coupling regime or merging with the cavity resonance in the Purcell regime are sensitive to input field at intermediate powers, and cannot be well described by the semiclassical approximation due to the quantum-dot saturation. As the GFR and GCB around the cavity resonance are relatively immune to the saturation effects, the rapid readout of single-electron spins can be carried out with coherent state and other statistically fluctuating light fields. This also shows that high-speed quantum entangling gates, robust against input power variations, can be built exploiting these linear effects.

DOI: 10.1103/PhysRevB.91.075304 PACS number(s): 78.67.Hc, 42.50.Pq, 78.20.Ek, 42.65.−k

I. INTRODUCTION

Semiconductor charged quantum dots (QDs) with confined electron or hole spins are promising for quantum computation [1–4], quantum communications [5–7], and quantum networks [8], especially for quantum internet with unconditional security [9]. Quantum gates are the key components for quantum information processing in an analog to the classical gates for classical information processing. To design deterministic quantum gates, three types of interactions can be exploited, i.e., photon-photon interactions [10–12], spin-spin interactions [13–18], and photon-spin interactions [19–24]. Although photons do not interact directly with each other intrinsically, photon-photon indirect interactions mediated by cavity QED have been demonstrated but are by definition nonlinear phenomena. For high photon-photon gate fidelity it is thus necessary to carefully control the "shape" of the overlapping photon wave packets to be top hat profiles. Direct spin-spin interactions suffer from short-range distance. Among the three types of interactions, the photon-spin interactions via optical transitions are the strongest and can be easily configured to mediate photon-photon and spin-spin (indirect) interactions for making various quantum gates with high speed.

Exploiting the cavity-QED enhanced photon-spin interactions, in our previous work we proposed two types of photon-spin entangling gates consisting of a single charged QD in an optical micro- or nanocavity for both quantum and classical information processing with high speed (tens to hundreds GHz) as well as for spin memory with heralded feature and unity efficiency [21,22,24]. The two types of photon-spin entangling gates are based on the giant optical Faraday rotation (GFR) and giant optical circular birefringence (GCB), which are induced by the single QD-confined spin in the cavity. GFR and GCB are manifested as large differences in the phase or amplitude of reflection/transmission coefficients between two circular polarizations of the input photons. Both phenomena can be regarded as the macroscopic imprint of the optical spin selection rules of the charged excitons in QDs.

However, in our previous work, the concepts of GFR and GCB were introduced in the weak-excitation approximation where the input field is in the low-power limit, and they can be regarded as the optical linear effects being independent of input power. In this work, we investigate how GFR and GCB can be extended from the weak-excitation approximation to the semiclassical approximation where the QD saturation effects induced by the input field are taken into account. An analytical method in the semiclassical approximation is adopted in comparison with the numerical calculations by the quantum optics toolbox [25].

We find that the semiclassical approximation can be used not only in the low- and high-power regimes, but also in a nonsaturation window around the cavity resonance in the strong-coupling regime at intermediate powers where the high cavity reflectivity leads to a higher saturation threshold. This higher saturation threshold leads to the retention of the linear effects into the intermediate-power regime around the cavity resonance. At frequencies close to the dressed state resonances, however, GFR and GCB become power dependent at lower powers and saturate earlier. Similar low-power saturation occurs in the Purcell regime where there is no dressed state splitting. The quantum gates based on the phase shifts (GFR) or reflection/transmission (GCB) around the cavity resonance are thus much less vulnerable to input power fluctuations.

This work is organized as follows: In Sec. II, we work out an analytical expression for the reflection coefficient in the semiclassical approximation in the type-I spin-cavity system consisting of a single QD spin in a single-sided optical cavity. The reflection amplitude and phase spectra are calculated using both the analytical method and Tan's quantum optics toolbox.

*chengyong.hu@bristol.ac.uk
†john.rarity@bristol.ac.uk

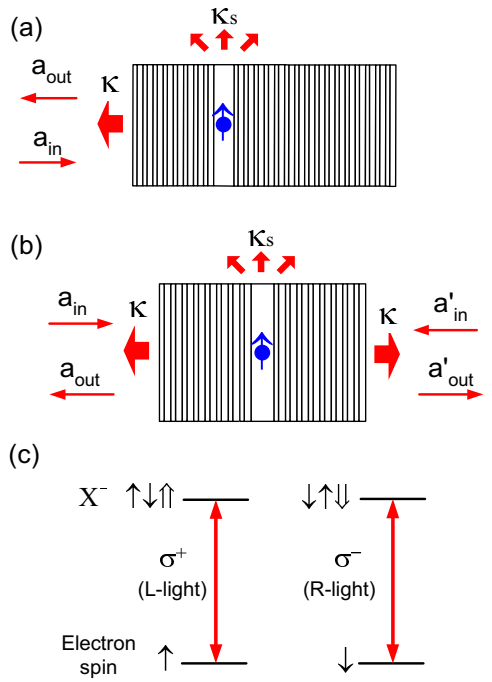

FIG. 1. (Color online) (a) Type-I spin-cavity system consisting of a QD spin in a single-sided cavity with one end mirror partially reflective and another end mirror 100% reflective. (b) Type-II spin-cavity system consisting of a QD spin in a double-sided cavity with both end mirrors partially reflective. The transmissions of the two mirrors are made symmetric to achieve maximal resonant transmission. (c) Optical spin selection rules for a negatively charged exciton X^- in QD. Only the vertical transitions are shown here as the weak cross transitions due to the heavy hole–light hole mixing can be corrected and are thus neglected here.

The regions of linear and nonlinear operation are identified and discussed. In Sec. III, we derive the analytical expressions for the reflection and transmission coefficients in the semiclassical approximation in the type-II spin-cavity system with the single QD spin in a double-sided optical cavity. The reflection and transmission spectra are calculated using both the analytical method and Tan's quantum optics toolbox. We identify and analyze the linear and nonlinear GCB. In Sec. IV, we show that the linear GFR and GCB around the cavity mode resonance are not affected by the high-order dressed state resonances. In Sec. V, we summarize our conclusions.

II. LINEAR AND NONLINEAR GFR IN TYPE-I SPIN-CAVITY SYSTEM

A negatively (or positively) charged QD has an excess electron (or hole) confined in the QD. Charging a QD can be achieved by modulation doping techniques or tunneling in *n-i-n* structures [26]. The ground states of charged QDs are two spin states of the excess electron (or the excess hole), and the excited states are two spin states of the negatively charged exciton X^- (or the positively charged exciton X^+) as shown in Fig. 1(c). Note that both the ground and the excited states are spin degenerate due to the Kramers theorem [27].

We consider such a charged QD embedded in a single-sided optical microcavity or nanocavity with the one end mirror partially reflective and another one 100% reflective [21]. The external light couples the system via the partially reflective end mirror. Figure 1(a) shows an experimental realization with the pillar microcavity where two distributed Bragg reflectors (DBRs) and transverse index guiding provide three-dimensional confinement of light. The cross section of the micropillar is made circular so that the cavity mode is frequency degenerate for two circular polarizations. Some photonic crystal nanocavities with specific symmetry (e.g., in Ref. [28]) can also support circularly polarized modes and are suitable for this work, too. The cavity mode frequency is designed to match the optical transition of the QD.

In this spin-cavity unit, there exists significant phase difference in the reflection coefficients between the "hot" and the "cold" cavity or between two circular polarizations of the input photons [21]. This GFR effect is a macroscopic manifestation of the optical spin selection rule of charged excitons [29] [see Fig. 1(c)] thanks to the cavity QED enhancement. The left circularly polarized photon (marked as L or σ^-) only couples the transition $|\uparrow\rangle \leftrightarrow |\uparrow\downarrow\uparrow\rangle$, and the right circularly polarized photon (marked as R or σ^+) only couples the transition $|\downarrow\rangle \leftrightarrow |\downarrow\uparrow\downarrow\rangle$. Here $|\uparrow\rangle$ and $|\downarrow\rangle$ represent electron spin states $|\pm\frac{1}{2}\rangle$, and $|\uparrow\rangle$ and $|\downarrow\rangle$ represent heavy-hole spin states $|\pm\frac{3}{2}\rangle$ with the spin quantization axis along the photon input direction. The photon polarizations are marked by the input states to avoid any confusion due to the temporary polarization changes upon reflection.

If the spin is in the state $|\uparrow\rangle$, the photon in the $|L\rangle$ state couples to the cavity mode and feels like a "hot" cavity, whereas the photon in the $|R\rangle$ state does not couple to the cavity mode and feels like a "cold" cavity. If the spin is in the state $|\downarrow\rangle$, the photon in the $|R\rangle$ state feels like a "hot" cavity and the photon in the $|L\rangle$ state feels like a "cold" cavity. The phase difference of the reflection coefficient between the cold and hot cavity is mapped to that between the two circular polarizations. Probing such a system with a linearly polarized light leads to giant Faraday rotations of the polarization directions of light (the GFR effect) [21].

In the following, we extend the concept of GFR from the weak-excitation approximation to the semiclassical approximation, and work out an analytical expression for the reflection coefficient of the hot and cold cavity with the QD saturation effects taken into account.

The Heisenberg equations of motions for the cavity field operator $\hat{a}$ and the QD dipole operators σ_-, σ_z, [30,31] together with the input-output relation [32], can be written as

$$\begin{aligned}
\frac{d\hat{a}}{dt} &= -\left[i(\omega_c-\omega)+\frac{\kappa}{2}+\frac{\kappa_s}{2}\right]\hat{a} - g\sigma_- - \sqrt{\kappa}\hat{a}_{\rm in},\\
\frac{d\sigma_-}{dt} &= -\left[i(\omega_{X^-}-\omega)+\frac{\gamma}{2}\right]\sigma_- - g\sigma_z\hat{a},\\
\frac{d\sigma_z}{dt} &= 2g(\sigma_+\hat{a}+\hat{a}^+\sigma_-) - \gamma_\parallel(1+\sigma_z),\\
\hat{a}_{\rm out} &= \hat{a}_{\rm in} + \sqrt{\kappa}\hat{a},
\end{aligned} \tag{1}$$

where ω, ω_c, ω_{X^-} are the frequencies of the input field, the cavity mode, and the X^- transition, respectively. g is the X^- cavity coupling strength [33]. $\gamma/2$ is the total QD dipole decay rate [34] which includes the spontaneous emission

induced decay rate $\gamma_\parallel/2$ and the pure dephasing rate γ^*; i.e., $\gamma/2 = \gamma_\parallel/2 + \gamma^*$. $\kappa/2$ is the the cavity field decay rate into the input/output port. $\kappa_s/2$ is the cavity field decay rate into the leaky modes due to side leakage, or other loss channels such as the material background absorption and possible losses in the highly reflective end mirror in practical situation.

If the correlations between the cavity field and the QD dipole are neglected (this is called the semiclassical approximation) [35,36], we have $\langle\sigma_\pm\hat{a}\rangle = \langle\sigma_\pm\rangle\langle\hat{a}\rangle$ and $\langle\sigma_z\hat{a}\rangle = \langle\sigma_z\rangle\langle\hat{a}\rangle$. The conditions to apply the semiclassical approximation will be discussed later. The reflection coefficient can thus be derived as

$$r(\omega) \equiv |r(\omega)|e^{i\phi(\omega)} = 1 - \frac{\kappa\left[i(\omega_{X^-} - \omega) + \frac{\gamma}{2}\right]}{\left[i(\omega_{X^-} - \omega) + \frac{\gamma}{2}\right]\left[i(\omega_c - \omega) + \frac{\kappa}{2} + \frac{\kappa_s}{2}\right] - g^2\langle\sigma_z\rangle}. \tag{2}$$

The population difference $\langle\sigma_z\rangle$ is given by

$$\langle\sigma_z\rangle = -\frac{1}{1 + \frac{\langle n\rangle}{n_c[1+4(\omega_{X^-}-\omega)^2/\gamma^2]}}, \tag{3}$$

and the average cavity photon number $\langle n\rangle \equiv \langle\hat{a}^\dagger\hat{a}\rangle$ by

$$\langle n\rangle = \frac{\kappa\left[(\omega_{X^-} - \omega)^2 + \frac{\gamma^2}{4}\right]P_{\rm in}}{\left[(\omega_{X^-} - \omega)^2 + \frac{\gamma^2}{4}\right]\left[(\omega_c - \omega)^2 + \frac{(\kappa+\kappa_s)^2}{4}\right] + 2g^2\langle\sigma_z\rangle\left[(\omega_{X^-} - \omega)(\omega_c - \omega) - \frac{(\kappa+\kappa_s)\gamma}{4}\right] + g^4\langle\sigma_z\rangle^2}, \tag{4}$$

where $n_c = \gamma_\parallel\gamma/8g^2$ is the critical photon number which measures the average cavity photon number required to saturate the QD response [37], and $n_c = 2.2\times10^{-4}$ is taken in this work. $P_{\rm in} = \langle\hat{a}_{\rm in}^\dagger\hat{a}_{\rm in}\rangle$ is the input field power. $\langle\sigma_z\rangle$ is the QD population difference between the excited state and the ground state, and can be used to measure the saturation degree. $\langle\sigma_z\rangle$ ranges from -1 to 0. If $\langle\sigma_z\rangle = -1$, the QD is in the ground state (not saturated); if $\langle\sigma_z\rangle = 0$, the QD is fully saturated, i.e., 50% probability in the ground states and 50% probability in the excited states. If $\langle\sigma_z\rangle$ takes other values, the QD is partially saturated.

By solving Eqs. (3) and (4), $\langle\sigma_z\rangle$ and $\langle n\rangle$ can be obtained at any input field strength [38]. Note that $\langle\sigma_z\rangle$ and $\langle n\rangle$ are dependent on the input power, the frequency, and the coupling strength g. Putting $\langle\sigma_z\rangle$ into Eq. (2), we can obtain both the amplitude and the phase of the reflection coefficient.

Alternatively, the reflection coefficient can be calculated numerically by the master equations in the Lindblad form with Tan's quantum optics toolbox [25]. The master equation for the spin-cavity system can be written as

$$\begin{aligned}\frac{d\rho}{dt} &= -i[H_{JC},\rho] + (\kappa+\kappa_s)\left(\hat{a}\rho\hat{a}^\dagger - \frac{1}{2}\hat{a}^\dagger\hat{a}\rho - \frac{1}{2}\rho\hat{a}^\dagger\hat{a}\right)\\ &\quad + \gamma_\parallel\left(\hat{\sigma}_-\rho\hat{\sigma}_+ - \frac{1}{2}\hat{\sigma}_+\hat{\sigma}_-\rho - \frac{1}{2}\rho\hat{\sigma}_+\hat{\sigma}_-\right)\\ &\quad + \frac{\gamma^*}{2}(\hat{\sigma}_z\rho\hat{\sigma}_z - \rho)\\ &\equiv \mathcal{L}\rho,\end{aligned} \tag{5}$$

where ρ is the reduced density matrix of the system, and all the parameters $\kappa,\kappa_s,\gamma,\gamma_\parallel,\gamma^*$ are defined in the same way as in Eq. (1). $\mathcal{L}$ is the Liouvillian and H_{JC} is the driven Jaynes-Cummings Hamiltonian with the input field driving the cavity. In the frame rotating at the input field frequency, H_{JC} can be written as

$$\begin{aligned}H_{JC} &= (\omega_c - \omega)\hat{a}^\dagger\hat{a} + (\omega_{X^-} - \omega)\sigma_+\sigma_-\\ &\quad + ig(\sigma_+\hat{a} - \hat{a}^\dagger\sigma_-) + i\sqrt{\kappa}\hat{a}_{\rm in}(\hat{a} - \hat{a}^\dagger),\end{aligned} \tag{6}$$

where the input field is associated with the output field and the cavity field by the input-output relation $\hat{a}_{\rm out} = \hat{a}_{\rm in} + \sqrt{\kappa}\hat{a}$ as described earlier.

Although the analytical solution to the master equation in Eq. (5) is difficult, Tan's quantum optics toolbox in MATLAB provides an exact numerical solution to the density matrix $\rho(t)$ or $\rho(t\to\infty)$ in steady state. By taking the operator average in the input-output relation, the reflection coefficient in the steady state can be calculated by the expression

$$r(\omega) = 1 + \sqrt{\kappa}\frac{{\rm Tr}(\rho\hat{a})}{\langle\hat{a}_{\rm in}\rangle}. \tag{7}$$

This method yields the reflection coefficient for arbitrary input states in principle. In this work we look at reflection coefficients for classical input fields (coherent states) or single-photon trains at different light intensities. The coherence times of these input fields are long compared to the cavity lifetime.

Next we study the reflection spectra calculated from the two methods described above. We focus on the results in the strong-coupling regime as from these results the information in the Purcell regime or weak-coupling regime can be extracted. Strongly coupled QD-cavity systems with $g > (\kappa+\kappa_s-\gamma)/4$ have been experimentally demonstrated in various micro- or nanocavities [39–41]. In this work we take $g = 2.4(\kappa+\kappa_s)$ which can be achieved for In(Ga)As QDs in the state-of-the-art pillar microcavity [39,42,43]. The side leakage rate κ_s depends on fabrication and various cavity details such as materials, structures, and size, and we take $\kappa_s = 0.5\kappa$ in our calculations. The total QD decay rate γ due to the spontaneous emission and the pure dephasing processes is sample dependent and it is usually smaller than the cavity decay rate $\kappa+\kappa_s$ in high-quality samples. The QD is tuned in resonance with the cavity mode; i.e., $\omega_{X^-} = \omega_c = \omega_0$.

Figures 2(a) and 2(b) show the reflectance $|r(\omega)|$ and phase $\phi(\omega)$ spectra of the hot cavity in the strong-coupling regime with $g/(\kappa+\kappa_s) = 2.4$ at different input powers. The input power is normalized by $(\kappa+\kappa_s)$ (i.e., in photons per cavity lifetime) where $\kappa+\kappa_s$ is the total cavity decay rate. At

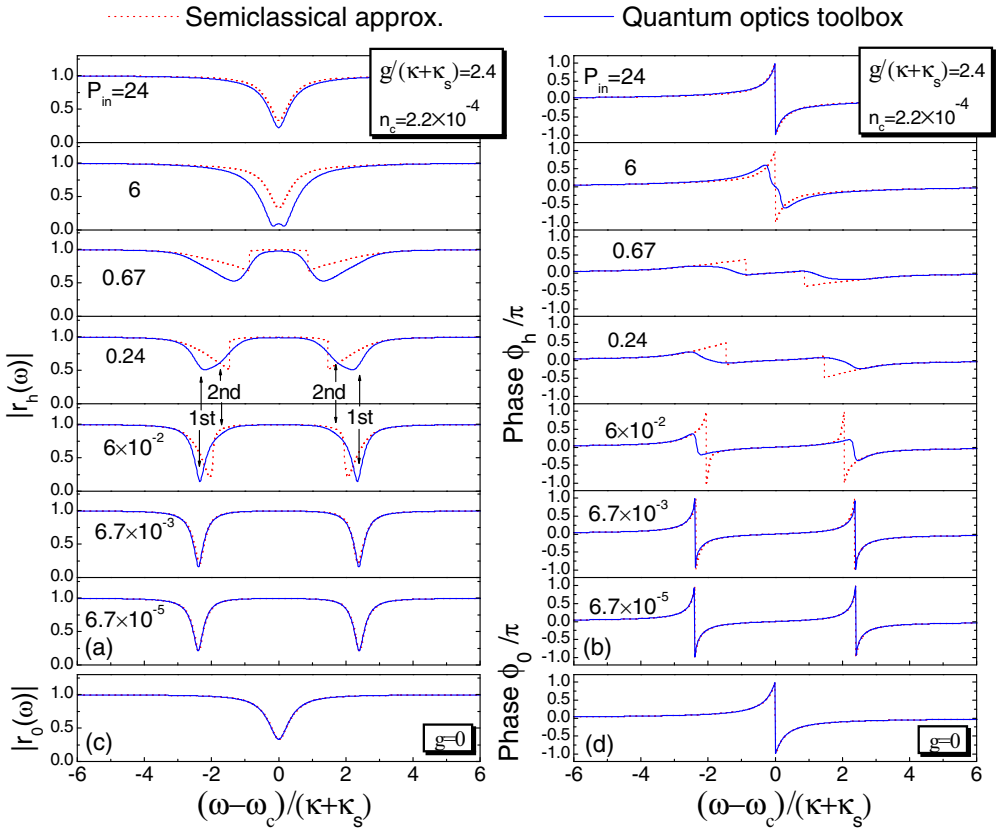

FIG. 2. (Color online) (a) Reflectance $|r_h(\omega)|$ spectra and (b) phase $\phi_h(\omega)$ spectra from a hot cavity with $g = 2.4(\kappa + \kappa_s)$ in the strong-coupling regime at different input field powers. The input power $P_{\rm in}$ is normalized by $\kappa + \kappa_s$ (i.e., in photons per cavity lifetime). (c) Reflectance $|r_0(\omega)|$ spectra and (d) phase $\phi_0(\omega)$ spectra from a cold cavity (with $g = 0$). Red dotted curves are calculated by using Eq. (2) in the semiclassical approximation, and blue solid curves are calculated by the quantum optics toolbox [25].

low powers ($P_{\rm in} < 0.026$ photons/cavity lifetime; low-power regime), the two dips observed in the reflectance spectra and the related two oscillating features in the phase spectra are due to the resonances of the first manifold of dressed states (also called polariton states or normal modes) separated by the vacuum Rabi splitting (or normal mode splitting) [44]. We note that the semiclassical approximation and the toolbox yield identical results.

With increasing input power ($0.026 < P_{\rm in} < 1.1$; intermediate-power regime), the two reflectance dips and phase features become weaker, and both shift towards the cavity resonance at ω_c (i.e., at the zero detuning $\omega - \omega_c = 0$). Moreover, there is obvious discrepancy on the reflectance dips and phase features between the two calculation methods. Further increasing the power ($P_{\rm in} > 1.1$; high-power regime), the two reflectance dips and phase features merge into one around the cavity resonance. Both the reflectance and the phase spectra of the hot cavity look similar to those of the cold cavity as shown in Figs. 2(c) and 2(d). We note that the power-dependent reflection spectra [45] were experimentally demonstrated recently [46–48].

The phase difference between the cold and hot cavity is an indication of the phase difference between two circular polarizations of the reflected photons if the spin is included (see discussions at the beginning of this section), which is the GFR effect. Figure 3(a) presents the phase difference $\phi_0(\omega) - \phi_h(\omega)$ spectra between the cold and the hot cavity at different input powers. Note that the GFR angle equals one-half of the phase difference. Besides the two oscillating phase features associated with the dressed state resonances, there is another oscillating feature around the cavity resonance. The third phase feature is mainly contributed by the cold cavity as the phase is nearly zero around the cavity frequency for the hot cavity as shown in Fig. 2(b). The strength of the third phase feature is not affected by the input field in the low- and intermediate-power regimes, but it disappears in the high-power regime. We also note that the semiclassical approximation works well for this phase feature as both calculations yield the same results. The other two phase features related to the dressed states shift toward the cavity resonance, merge into one, and finally disappear with increasing the input power in the intermediate- and high-power regimes. For these two phase features, there are significant discrepancies between the semiclassical approximation and the toolbox.

The above results can be explained by the QD saturation induced by the input field. The saturation spectra are shown in Fig. 3(b). In the low-power regime ($P_{\rm in} \ll 1$), the saturation effect can be neglected as the QD is almost in the ground state; i.e., $\langle \sigma_z \rangle \simeq -1$ in the whole frequency range. This is exactly the weak-excitation approximation used in our previous work [21,22]. As there is no real excitation, there are no correlations between the cavity field and the QD

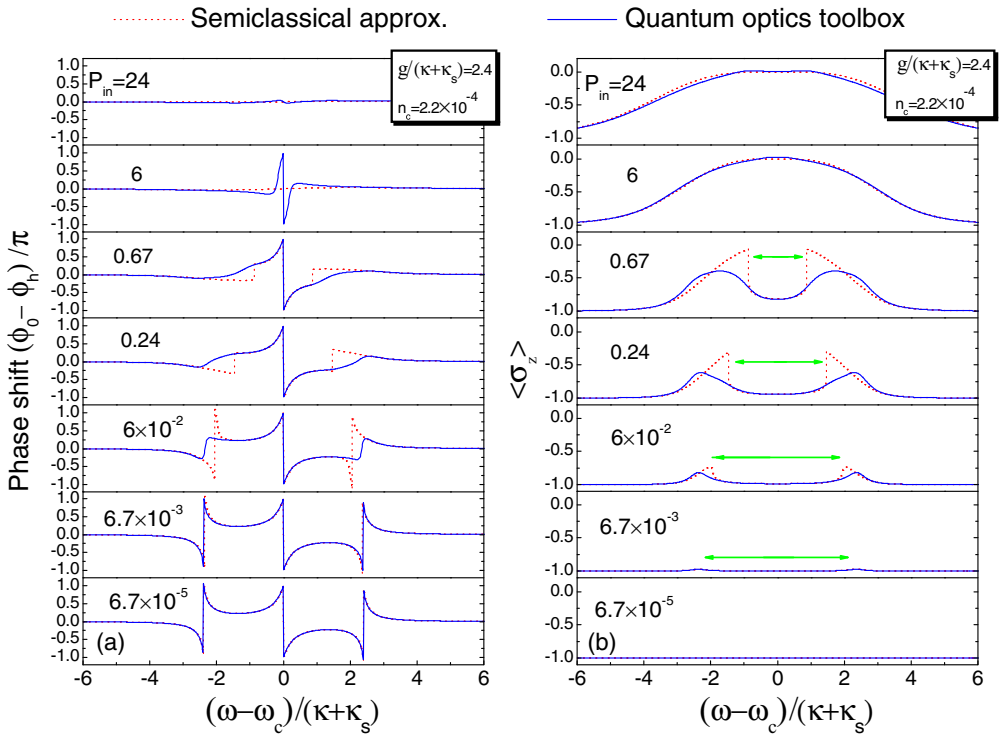

FIG. 3. (Color online) (a) Phase shift $\phi_0(\omega)-\phi_h(\omega)$ spectra between the cold cavity with $g=0$ and the hot cavity with $g=2.4(\kappa+\kappa_s)$ at different input powers. The GFR angles equal one-half of the phase shift. (b) The QD saturation curves at different input powers. The nonsaturation windows (marked by green arrows) are observed between two dressed state resonances at intermediate powers. The input power is normalized by $\kappa+\kappa_s$ (i.e., in photons per cavity lifetime). Red dotted curves are calculated by using Eq. (2) in the semiclassical approximation, and blue solid curves are calculated by the quantum optics toolbox.

dipole, and the assumption $\langle\sigma_{\pm,z}\hat{a}\rangle=\langle\sigma_{\pm,z}\rangle\langle\hat{a}\rangle$ is valid. The semiclassical approximation is then equivalent to the weak-excitation approximation in the low-power regime. This explains why the reflectance, the phase, and the phase shift or GFR spectra are not affected by input field at low powers.

In the intermediate-power regime ($P_{\rm in}\sim1$), the input field in resonance with the dressed states can enter the cavity and build the cavity field which saturates the QD. The QD saturation reduces the QD-cavity coupling strength to $g_{\rm eff}=g\sqrt{|\langle\sigma_z\rangle|}$, so the Rabi splitting becomes smaller and the dressed states shift toward the cavity resonance frequency with increasing input powers ($\langle\sigma_z\rangle$ from -1 to 0) (see Figs. 2 and 3). The phase difference (or GFR) associated with the dressed state resonance is nonlinear as both the strength and the frequency vary with the input field. There are significant correlations between the QD dipole and the cavity fields, so the semiclassical approximation does not work well for this nonlinear GFR associated with the dressed state resonances.

However, in the intermediate-power regime the saturation effect remains weak around $\omega=\omega_c$ [see Fig. 3(b)]. The cavity resonance is a highly reflective region [see Fig. 2(a)] which prevents photons from entering the cavity and saturating the QD effectively. Therefore, the QD remains in the ground states; i.e., $\langle\sigma_z\rangle\simeq-1$. In this nonsaturation window, the semiclassical approximation still works well, and yields the same results as the toolbox. The GFR spectra in the nonsaturation window are not affected by the input power, and remain the same strength as those in the low-power limit except the window size shrinks with increasing input power. The GFR within the nonsaturation window is therefore a linear effect.

In the high-power regime ($P_{\rm in}\gg1$), the saturation effect becomes so strong that the nonsaturation window is closed [49] and the QD is fully saturated; i.e., $\langle\sigma_z\rangle\simeq0$. The full saturation starts from the center of the cavity resonance and extends towards its two sides. The cavity with a saturated QD behaves like a cold cavity, so the phase difference between the hot and cold cavity disappears [see Fig. 3(a)].

Besides the evolution of the nonsaturation window, from the saturation spectra we also observe the power or saturation broadening of the QD response with increasing the input power [50].

Figure 4(a) presents GFR at a fixed frequency close to the cavity resonance (within the nonsaturation window) as a function of input power. The phase difference of $\pi/2$ is chosen as the $\pi/2$ phase shift is required for making the ideal photon-spin entangling gates [21]. We see that GFR is constant with the input power up to $P_{\rm in}\simeq1$ in accordance with the calculations [49]. In this region, the reflectance is also independent of the input power as shown in Fig. 4(b). As a result, the photon-spin entangling gate (see Ref. [21]) based on this linear GFR is resistant to the photon rate variations, which is highly desirable in practical applications such as quantum communications and quantum computation. Again it is verified that the semiclassical approximation works well for the linear GFR as it yields results identical to those of the toolbox. In contrast, the GFR related to the dressed state resonances starts saturating at much lower powers [see Fig. 3(a)].

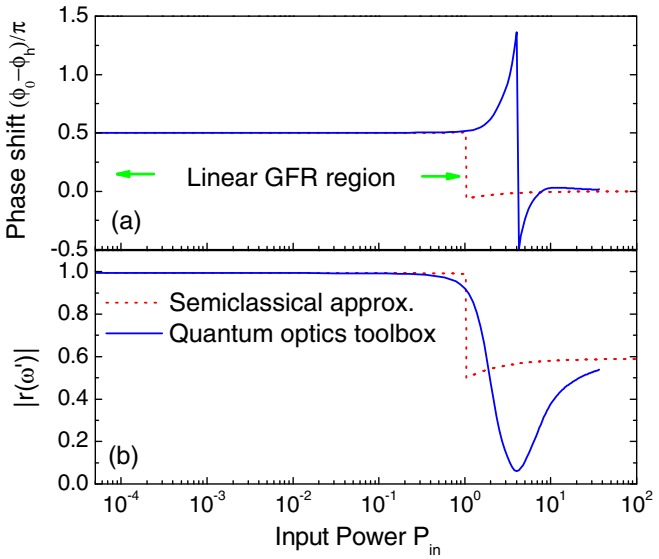

FIG. 4. (Color online) (a) The linear phase shift (corresponding to the linear GFR) as a function of the input power. The phase shift is tracked at a fixed frequency within the nonsaturation window. Here we choose a phase shift of $\pi/2$, corresponding to a GFR angle of $\pi/4$. (b) The reflectance as a function of the input power. The reflectance is tracked at a fixed frequency which is the same as in (a). The input power is normalized by $\kappa+\kappa_s$ (i.e., in photons per cavity lifetime). Red dotted curves show results calculated from the semiclassical approximation, and blue solid curves are calculated by the quantum optics toolbox.

The large fluctuations of GFR at the start of the high-power regime (see Fig. 4) are due to the nonlinear GFR. When the input power increases from the intermediate- to the high-power regime, the saturation induces a transition from the strong-coupling to weak-coupling regime at an input power where the nonsaturation window is closed and the linear GFR was eaten up by the nonlinear GFR. This also takes place in the conventional Purcell regime with $\gamma < 4g^2/(\kappa+\kappa_s) < (\kappa+\kappa_s)$ where no linear GFR exists and the cavity resonance region is covered by the nonlinear GFR that is vulnerable to the input field power (the results are not shown here). When the QD saturation occurs over a large frequency range, the nonlinear GFR disappears as well. Similarly, in the weak-coupling regime $4g^2/(\kappa+\kappa_s) < \gamma$, the concept of the "one-dimensional atom" breaks down and no GFR exists. Instead, the conventional Faraday rotation enhanced by the cavity (due to the back and forth propagation of light in the cavity) can be observed with the rotation angles at least five orders of magnitude smaller than the GFR angles. Note that GFR is enhanced by the cavity QED [21], rather than the cavity only.

III. LINEAR AND NONLINEAR GCB IN TYPE-II SPIN-CAVITY SYSTEM

In this section, we consider the type-II spin-cavity unit with a charged QD in a double-sided optical microcavity where the two end mirrors are both partially reflective [see Fig. 1(b)]. In this spin cavity-QED system, the GCB manifests as the different reflection/transmission coefficients between the cold and hot cavity or between the R- and L-circular polarizations of input photons. This allows us to make another photon-spin entangling gate, i.e., the entanglement beam splitter [22], which can directly split a spin-photon polarization product state into two constituent entangled states.

The reflection or transmission behaviors in similar systems were investigated in the weak-coupling regime in either the weak-excitation approximation [51–53] or in the semiclassical approximation [53,54]. To derive the reflection and transmission coefficients in the strong-coupling regime with the QD saturation taken into account, we apply the same approach as discussed in Sec. II, i.e., the Heisenberg equations of motion for the cavity field operator $\hat{a}$ and the QD dipole operators σ_- and σ_z [30,31], together with the input-output relations [32],

$$\begin{aligned}
\frac{d\hat{a}}{dt} &= -\left[i(\omega_c-\omega)+\kappa+\frac{\kappa_s}{2}\right]\hat{a}-g\sigma_- -\sqrt{\kappa}\hat{a}_{\rm in}-\sqrt{\kappa}\hat{a}'_{\rm in},\\
\frac{d\sigma_-}{dt} &= -\left[i(\omega_{X^-}-\omega)+\frac{\gamma}{2}\right]\sigma_- - g\sigma_z\hat{a},\\
\frac{d\sigma_z}{dt} &= 2g(\sigma_+\hat{a}+\hat{a}^+\sigma_-)-\gamma_\parallel(1+\sigma_z),\\
\hat{a}_{\rm out} &= \hat{a}_{\rm in}+\sqrt{\kappa}\hat{a},\\
\hat{a}'_{\rm out} &= \hat{a}'_{\rm in}+\sqrt{\kappa}\hat{a}.
\end{aligned} \tag{8}$$

All the parameters here have the same definitions and meanings as in Eq. (1).

Following a procedure similar to that in Sec. II, the analytical expressions for the reflection and transmission coefficients can be derived in the semiclassical approximation by neglecting the correlations between the cavity field and the QD dipole; i.e.,

$$\begin{aligned}
r(\omega) &= 1+t(\omega),\\
t(\omega) &= \frac{-\kappa\left[i(\omega_{X^-}-\omega)+\frac{\gamma}{2}\right]}{\left[i(\omega_{X^-}-\omega)+\frac{\gamma}{2}\right]\left[i(\omega_c-\omega)+\kappa+\frac{\kappa_s}{2}\right]-g^2\langle\sigma_z\rangle}.
\end{aligned} \tag{9}$$

The semiclassical approximation works well in three situations: (1) low-power limit in the weak- or strong-coupling regime; (2) high-power limit in the weak- or strong-coupling regime; (3) within the nonsaturation window in the strong-coupling regime. These conditions to apply the semiclassical approximation are the same for both types of spin-cavity systems.

The average population $\langle\sigma_z\rangle$ is given by Eq. (3) and the average cavity photon number $\langle n\rangle$ by

$$\langle n\rangle = \frac{\kappa\left[(\omega_{X^-}-\omega)^2+\frac{\gamma^2}{4}\right]P_{\rm in}}{\left[(\omega_{X^-}-\omega)^2+\frac{\gamma^2}{4}\right]\left[(\omega_c-\omega)^2+\frac{(2\kappa+\kappa_s)^2}{4}\right]+2g^2\langle\sigma_z\rangle\left[(\omega_{X^-}-\omega)(\omega_c-\omega)-\frac{(2\kappa+\kappa_s)\gamma}{4}\right]+g^4\langle\sigma_z\rangle^2}, \tag{10}$$

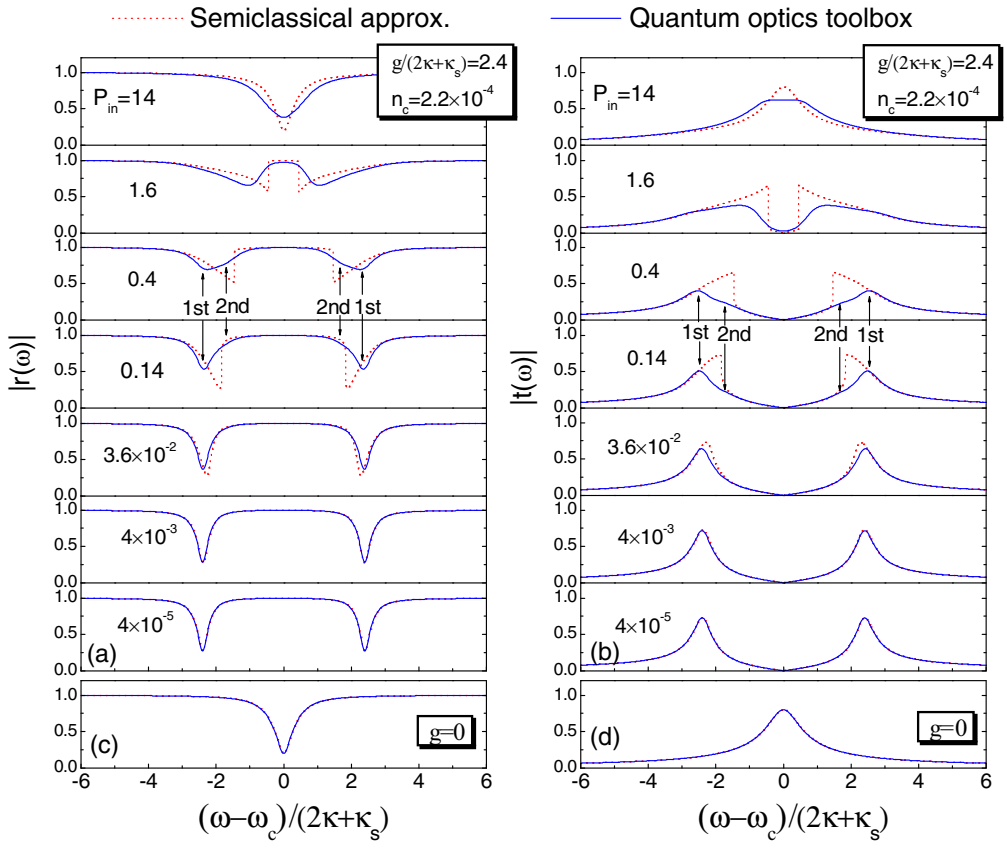

FIG. 5. (Color online) (a) Reflectance $|r_h(\omega)|$ spectra and (b) transmittance $|t_h(\omega)|$ spectra from a hot cavity in the strong-coupling regime with $g = 2.4(2\kappa + \kappa_s)$ at different input field powers. (c) Reflectance $|r_0(\omega)|$ spectra and (d) transmittance $|t_0(\omega)|$ spectra from a cold cavity ($g = 0$). The input powers are normalized by $2\kappa + \kappa_s$ (i.e., in photons per cavity lifetime). Red dotted curves are calculated by using Eq. (9) in the semiclassical approximation, and blue solid curves are calculated by the quantum optics toolbox.

where the critical photon number n_c is defined in the same way as in Sec. II.

From Eqs. (3) and (10), both $\langle\sigma_z\rangle$ and $\langle n\rangle$ can be calculated at any given input field strength. Putting $\langle\sigma_z\rangle$ into Eq. (9), we can obtain the reflection and transmission coefficients. Alternatively, the reflection and transmission coefficients can be calculated numerically in the frame of the master equation using Tan's quantum optics toolbox with the same technique as described in Sec. II. From the obtained density matrix ρ in steady state and the input-output relations, the reflection and transmission coefficients can be calculated by the expressions

$$r(\omega) = 1 + t(\omega), \quad t(\omega) = \sqrt{\kappa}\frac{\mathrm{Tr}(\rho\hat{a})}{\langle\hat{a}_{\mathrm{in}}\rangle}. \tag{11}$$

We use the above two methods to study the GCB in this spin-cavity system.

Figures 5(a) and 5(b) show the reflectance $|r(\omega)|$ and the transmittance $|t(\omega)|$ spectra of the hot cavity in the strong-coupling regime with $g/(2\kappa + \kappa_s) = 2.4$ at different input powers. The reflection or transmission coefficients are different between the hot [see Figs. 5(a) and 5(b)] and the cold cavity [see Figs. 5(c) and 5(d)], indicating the reflection or transmission difference between the two circular polarizations of the input photons, which is the GCB effect [22]. Note that the reflection or transmission coefficients of the cold cavity [see Figs. 5(c) and 5(d)] are input power independent, so the reflection or transmission coefficients of the hot cavity can stand alone to represent the GCB effect [see Figs. 5(a) and 5(b)].

Following the similar discussions in Sec. II, we identify both linear and nonlinear GCB in this spin-cavity unit. The linear GCB lies within the nonsaturation window around the cavity resonance and is manifested as nearly unity reflectance and nearly zero transmission from the hot cavity. The linear GCB does not depend on the input power in the low- ($P_{\mathrm{in}} < 0.015$) and intermediate-power regime $0.015 < P_{\mathrm{in}} < 1.7$ as the QD saturation within the nonsaturation window is negligibly small. However, the linear GCB disappears at the start of the high-power regime $P_{\mathrm{in}} > 1.7$ where the nonsaturation window is closed [49].

The nonlinear GCB is associated with the dressed state resonances separated by the vacuum Rabi splitting. It is manifested as the two dips in the reflection spectra and two peaks in the transmission spectra. With increasing input power, the QD saturation becomes significant, so the two reflection dips and the two transmission peaks weaken and shift towards the cavity resonance. When the two reflection dips and the two transmission peaks merge into one dip or peak, the QD is fully saturated and the hot cavity turns to a cold cavity. As a result, the nonlinear GCB disappears. We see that the input field induces a transition from the strong-coupling to Purcell regime and finally to the weak-coupling regime. This transition

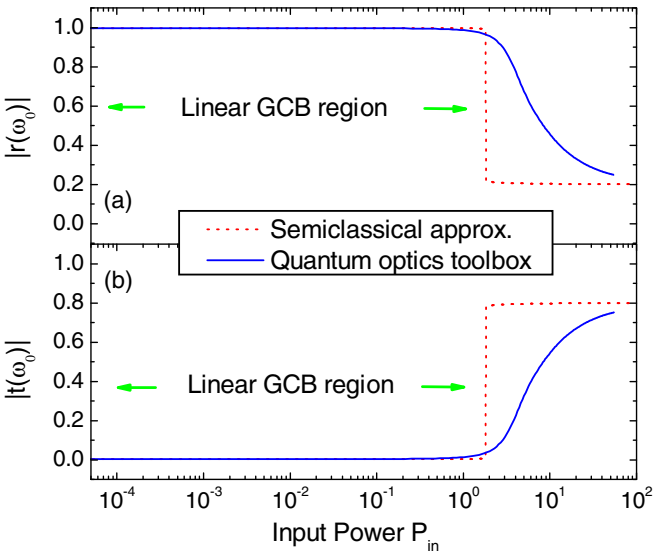

FIG. 6. (Color online) Reflectance and transmittance at $\omega = \omega_c$ from the hot cavity as a function of the input power. Note that the reflectance or transmittance from the cold cavity are independent of input power (not shown here). The input powers are normalized by $2\kappa + \kappa_s$ (i.e., in photons per cavity lifetime). Red dotted curves show results from the semiclassical approximation, and blue solid curves are calculated by the quantum optics toolbox.

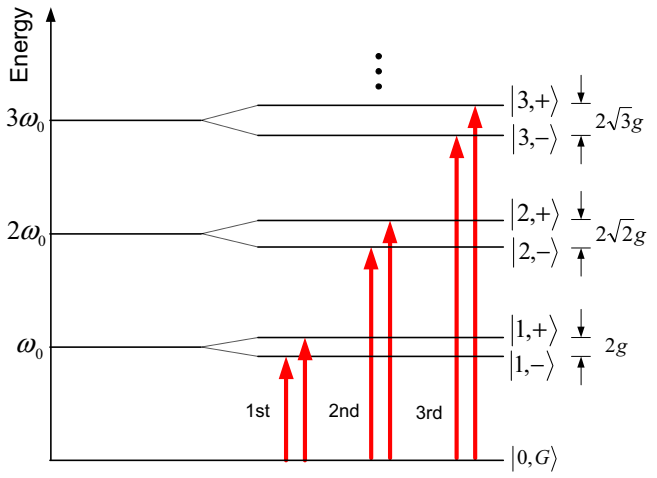

FIG. 7. (Color online) The Jaynes-Cummings energy spectrum and n-photon transitions from the ground state $|0,G\rangle$ to the dressed states $|n,\pm\rangle$. These high-order, multiphoton transitions can be observed in reflection or transmission spectra under some conditions as discussed in text. Dissipation processes are neglected in this diagram.

also happens in the type-I spin-cavity unit as discussed in Sec. II.

The linear GCB as a function of the input power is presented in Figs. 6(a) and 6(b). In the low- and intermediate-power regimes, the reflectance $|r(\omega_0)|$ and the transmittance $|t(\omega_0)|$ at the center of the cavity resonance remain constant with increasing input power up to $P_{\rm in} \simeq 1.7$ in accordance with the calculations [49]. Similar to the linear GFR discussed in Sec. II, the quantum gates built from the linear GCB are robust against the variations of input power or input photon rate.

In the Purcell regime $[\gamma < 4g^2/(2\kappa + \kappa_s) < 2\kappa + \kappa_s]$, the cavity resonance region is covered by the nonlinear GCB and there exists no linear GCB. As the nonlinear GCB is input power dependent, the quantum gates based on the nonlinear GCB are fragile when the input power varies. In the weak-coupling regime $4g^2/(2\kappa + \kappa_s) < \gamma$ where the concept of the "one-dimensional atom" (Ref. [31]) breaks down, there is no GCB effect. It is interesting to note that the concept of the "one-dimensional atom" can be partially recovered by placing the QD or atom in one-dimensional waveguides. However, the GCB expected in this waveguide structures is a nonlinear effect; therefore it is sensitive to the QD saturation or the input power.

IV. INFLUENCE OF HIGH-ORDER DRESSED STATES ON LINEAR GFR AND GCB

All results presented in previous sections are calculated in the strong-coupling regime with $g/(\kappa + \kappa_s) = 2.4$ for a single-sided cavity [or $g/(2\kappa + \kappa_s) = 2.4$ for a double-sided cavity] which can be experimentally achieved. The two reflection dips or two transmission peaks are explained as the first-order dressed state resonances, i.e., the transitions $|0,G\rangle \rightarrow |1,\pm\rangle$ where $|0,G\rangle$ is the ground state, and $|1,\pm\rangle$ is the first-order dressed states with $n = 1$ excitation [44]. In the strong-coupling regime, we also expect high-order dressed state resonances $|0,G\rangle \rightarrow |n,\pm\rangle$ (see Fig. 7). These dressed states build the anharmonic energy level diagram described by the Jaynes-Cummings ladder [55] which is regarded as an indication of the quantum nature of light-matter interactions. In Figs. 2 and 5 only very weak resonances related to the $n = 2$ dressed states are identified in the reflection and transmission spectra when the input power is around $P_{\rm in} = 0.1$–0.4, and resonance peaks related to high-order dressed states ($n > 2$) are washed out by the QD saturation, the cavity photon probability distribution, and the resonance broadening.

From Eqs. (3) and (4), we see that around the dressed state resonances or the cavity resonance the QD becomes less saturated and there are fewer photons accumulated in the cavity with increasing the coupling strength (if the input power is kept the same). At higher coupling strength, we clearly observe the high-order dressed state resonances around the two edges of the nonsaturation window. The larger the coupling strength, the more dressed state resonances can be observed. Although these large coupling strengths $g/(\kappa + \kappa_s)$ for QD-cavity systems go beyond the current state-of-the-art value $g/(\kappa + \kappa_s) = 2.7$ [43], this deeper strong-coupling regime allows us to investigate whether or not these high-order dressed states affect the linearity of GFR and GCB, and meanwhile get more insight into the spin-cavity QED systems.

Figure 8 presents the reflection and phase shift spectra at different input powers for a single-sided spin-cavity system with $g/(\kappa + \kappa_s) = 9.6$. The $n = 1,2,3$ dressed states are identified in reflection spectra calculated by the toolbox, but not by the semiclassical model. The first manifold of dressed states are observed for input powers below $P_{\rm in} = 9$, and the second manifold for input powers between $P_{\rm in} = 0.07$ and $P_{\rm in} = 9$, and the third manifold between $P_{\rm in} = 1.3$ and $P_{\rm in} = 9$. The dressed state resonances shift towards the cavity

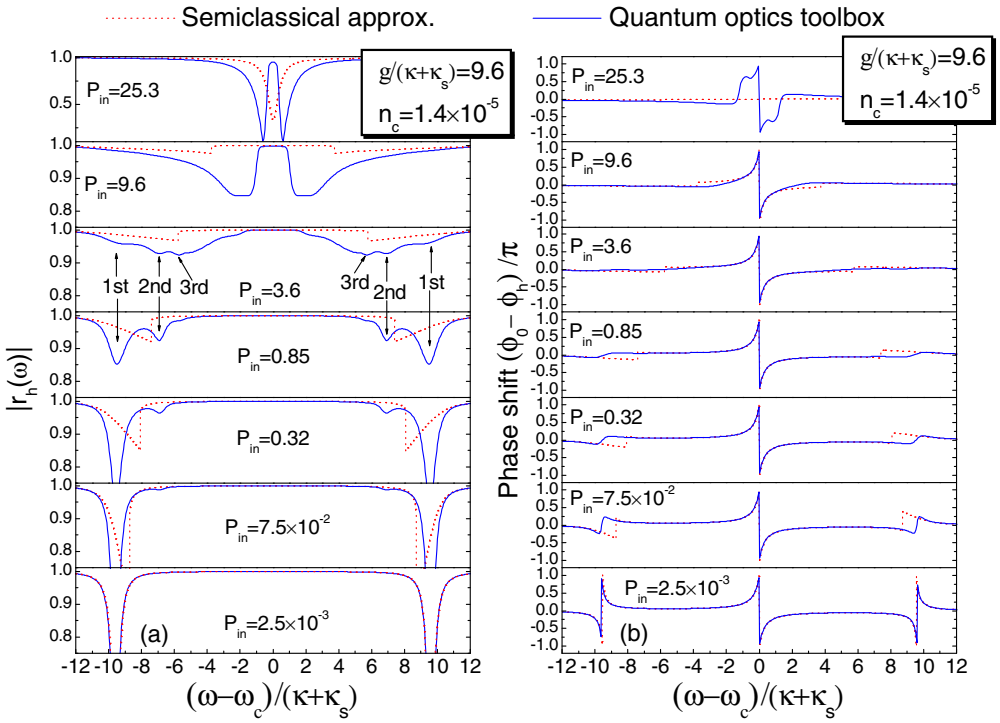

FIG. 8. (Color online) (a) Reflectance $|r_h(\omega)|$ spectra and (b) phase $\phi_h(\omega)$ spectra from a hot cavity with $g = 9.6(\kappa + \kappa_s)$ in the strong-coupling regime at different input field powers. The input power $P_{\rm in}$ is normalized by $\kappa + \kappa_s$ (i.e., in photons per cavity lifetime). The first, second, and third manifold of dressed states are observed in certain power range. Red dotted curves are calculated by using Eq. (2) in the semiclassical approximation, and blue solid curves are calculated by the quantum optics toolbox.

resonance with increasing the order n, and satisfy the resonance condition $n\omega = \omega_{n,\pm}$ where ω is the frequency of input field and $\omega_{n,\pm}$ are the energy eigenvalues of the nth-order dressed states. By diagonalization of the Liouvillian defined in Eq. (5), $\omega_{n,\pm}$ can be derived as $\omega_{n,\pm} = n\omega_0 - i[(2n-1)(\kappa+\kappa_s)+\gamma]/4 \pm \sqrt{ng^2 - [(\kappa+\kappa_s-\gamma)/4]^2}$ under the weak-excitation condition at zero detuning. As these dressed states $|n,\pm\rangle \simeq (|n,G\rangle \pm |n-1,E\rangle)/\sqrt{2}$ are highly entangled states between QD and cavity field, it is not surprising that the corresponding dressed state resonances cannot be observed in the reflection spectra calculated by the semiclassical model which neglects the correlation between QD and the cavity field (see Fig. 8) [44].

As all the dressed state resonances are situated around the edges of the nonsaturation window, the linear phase shift or the linear GFR around the cavity mode resonance are not affected by these dressed state resonances [see Fig. 8(b)] and persist up to $P_{\rm in} \simeq 20$ in accordance with calculations [49]. We notice that these dressed state resonances are observed only in a limited power range. The input field should be strong enough to inject enough photons into the cavity so that the occupation of $|n,G\rangle$ and $|n-1,E\rangle$ states can develop. Meanwhile, the input light should not be too strong to saturate the n-photon transitions $|0,G\rangle \rightarrow |n,\pm\rangle$. The higher the order of the dressed states, the smaller this power range and the more difficult to observe the dressed state resonances. Within this power range, the dressed state resonances remain in the same energy position. However, they become broader and get saturated finally, and after that all of them merge to two broad resonances which shift towards the cavity resonance with increasing input power. This can be explained by the QD saturation which reduces the coupling strength g to $g_{\rm eff} = g\sqrt{|\langle\sigma_z\rangle|}$ as discussed in Sec. II.

Figure 9 shows the reflection and transmission spectra at different input powers for a double-sided spin-cavity system with $g/(2\kappa+\kappa_s) = 9.6$. The $n = 1,2,3$ dressed state resonances are again identified in the reflection and transmission spectra calculated by the toolbox. The reflection and transmission around the cavity resonance, i.e., the linear GCB, are not affected by the higher-order dressed state resonances with increasing the power up to $P_{\rm in} \simeq 40$ in accordance with calculations [49].

Based on the discussions above, we can conclude that the linear GFR and GCB are robust against the multiphoton transitions (besides the QD saturation) up to a high power where the nonsaturation window is closed [49]. It is quite tricky to observe these high-order dressed state resonances. Besides the requirements of strong coupling and the resonance condition $n\omega = \omega_{n,\pm}$, lower saturation, higher coupling strength, and the right power range also need to be taken into account. Detailed discussions on these criteria to observe these multiphoton transitions are lengthy and go beyond the scope of this work, and will be published elsewhere [56].

V. CONCLUSIONS

We have studied the saturation nonlinear effects in QD-spin coupled cavity QED systems using an analytical approach in the semiclassical approximation compared with a numerical approach using Tan's quantum optics toolbox. We find that

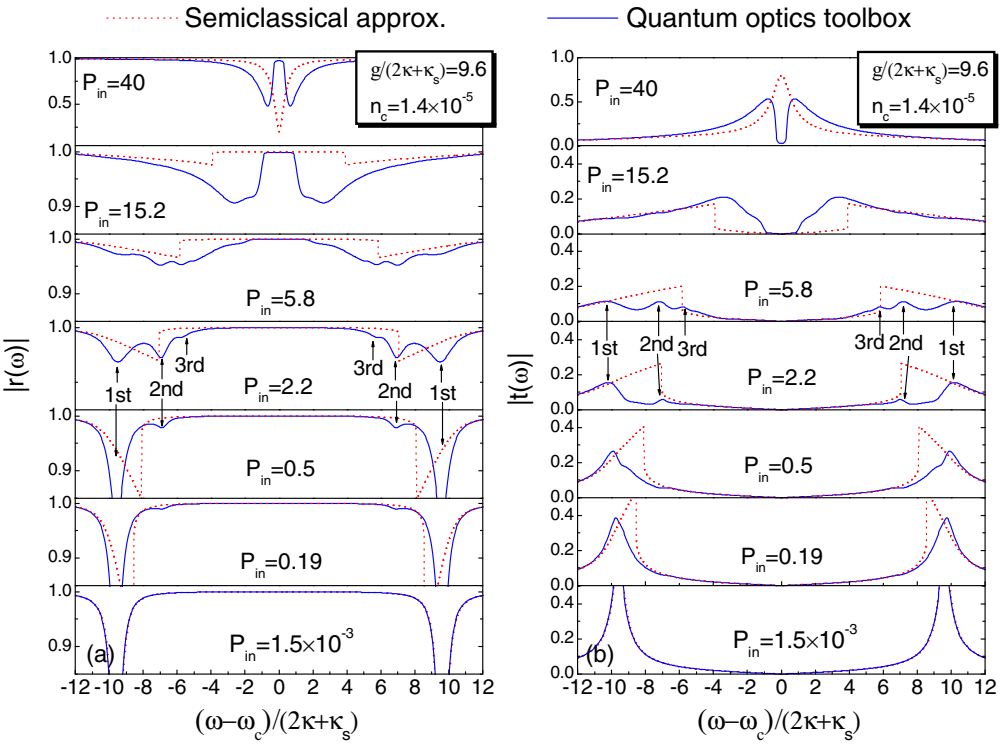

FIG. 9. (Color online) (a) Reflectance $|r_h(\omega)|$ spectra and (b) transmittance $|t_h(\omega)|$ spectra from a hot cavity in the strong-coupling regime with $g = 9.6(2\kappa + \kappa_s)$ at different input field powers. The input power $P_{\rm in}$ is normalized by $\kappa + \kappa_s$ (i.e., in photons per cavity lifetime). The first, second, and third manifolds of dressed states are observed in a certain power range. Red dotted curves are calculated by using Eq. (9) in the semiclassical approximation, and blue solid curves are calculated by the quantum optics toolbox.

the semiclassical approximation can be used not only in the low-power regime ($P_{\rm in} \ll 1$) and high-power regime ($P_{\rm in} \gg 1$), but also at intermediate powers ($P_{\rm in} \sim 1$) in a nonsaturation window between the two dressed-state resonances. In the low-power regime where the QD is in the ground state and the saturation is negligibly small, the semiclassical approximation is equivalent to the weak-excitation approximation where the GFR and GCB are linear effects across the whole frequency range.

The dressed state resonances saturate when the incident field contains much less than one photon per cavity lifetime leading to saturation nonlinearity in the associated GFR and GCB. Between the dressed state resonances (i.e., within the nonsaturation window) the saturation occurs at much higher incident photon rate (at a level of one photon per cavity lifetime) and we can see power-independent, linear GFR and GCB around the cavity resonance in the strong-coupling regime, which are robust against the QD saturation and multiphoton transitions. The higher the coupling strength g, the higher powers the linear effects can retain up to [49]. In the Purcell regime there is no dressed state splitting and thus no nonsaturation window and no linear effects exist. We conclude that the quantum gates [21,22] built from the linear effects either in the strong-coupling regime or in the low-power limit are robust against the input field intensity fluctuations, and can be safely applied for high-speed quantum and classical information processing with varying photon rates.

The fact that there is a lower nonlinear threshold for the dressed states suggests one could modify a relatively high-power on-resonance beam using a lower-power beam resonant with the dressed states. We are studying this "transistor" action and will present it in a separate paper.

ACKNOWLEDGMENTS

We acknowledge stimulating discussions with J. Adcock and T. D. Galley. This work is funded by ERC advanced grant QUOWSS (No. 247462) and ERANET/EPSRC project SSQN.

[1] M. A. Nielson and I. L. Chuang, *Quantum Computation and Quantum Information* (Cambridge University Press, Cambridge, 2000).

[2] T. D. Ladd, F. Jelezko, R. Laflamme, Y. Nakamura, C. Monroe, and J. L. O'Brien, Nature (London) **464**, 45 (2010).

[3] R.-B. Liu, W. Yao, and L. J. Sham, Adv. Phys. **59**, 703 (2010).

[4] D. D. Awschalom, L. C. Bassett, A. S. Dzurak, E. L. Hu, and J. R. Petta, Science **339**, 1174 (2013).

[5] N. Gisin, G. Ribordy, W. Tittel, and H. Zbinden, Rev. Mod. Phys. **74**, 145 (2002).

[6] V. Scarani, H. Bechmann-Pasquinucci, N. J. Cerf, M. Dušek, N. Lütkenhaus, and M. Peev, Rev. Mod. Phys. **81**, 1301 (2009).

[7] J.-W. Pan, Z.-B. Chen, C.-Y. Lu, H. Weinfurter, A. Zeilinger, and M. Żukowski, Rev. Mod. Phys. **84**, 777 (2012).

[8] J. I. Cirac, P. Zoller, H. J. Kimble, and H. Mabuchi, Phys. Rev. Lett. **78**, 3221 (1997).

[9] H. J. Kimble, Nature (London) **453**, 1023 (2008).

[10] Q. A. Turchette, C. J. Hood, W. Lange, H. Mabuchi, and H. J. Kimble, Phys. Rev. Lett. **75**, 4710 (1995).

[11] A. Imamoglu, H. Schmidt, G. Woods, and M. Deutsch, Phys. Rev. Lett. **79**, 1467 (1997).

[12] K. M. Gheri, K. Ellinger, T. Pellizzari, and P. Zoller, Fortschr. Phys. **46**, 401 (1998).

[13] D. Loss and D. P. DiVincenzo, Phys. Rev. A **57**, 120 (1998).

[14] A. Imamoglu, D. D. Awschalom, G. Burkard, D. P. DiVincenzo, D. Loss, M. Sherwin, and A. Small, Phys. Rev. Lett. **83**, 4204 (1999).

[15] C. Piermarocchi, P. Chen, L. J. Sham, and D. G. Steel, Phys. Rev. Lett. **89**, 167402 (2002).

[16] M. Feng, I. D'Amico, P. Zanardi, and F. Rossi, Phys. Rev. A **67**, 014306 (2003).

[17] T. Calarco, A. Datta, P. Fedichev, E. Pazy, and P. Zoller, Phys. Rev. A **68**, 012310 (2003).

[18] S. M. Clark, Kai-Mei C. Fu, T. D. Ladd, and Y. Yamamoto, Phys. Rev. Lett. **99**, 040501 (2007).

[19] L.-M. Duan and H. J. Kimble, Phys. Rev. Lett. **92**, 127902 (2004); A. Reiserer, N. Kalb, G. Rempe, and S. Ritter, Nature (London) **508**, 237 (2014); T. G. Tiecke, J. D. Thompson, N. P. de Leon, L. R. Liu, V. Vuletić, and M. D. Lukin, *ibid.* **508**, 241 (2014).

[20] W. Yao, R.-B. Liu, and L. J. Sham, Phys. Rev. Lett. **95**, 030504 (2005).

[21] C. Y. Hu, A. Young, J. L. O'Brien, W. J. Munro, and J. G. Rarity, Phys. Rev. B **78**, 085307 (2008); C. Y. Hu, W. J. Munro, and J. G. Rarity, *ibid.* **78**, 125318 (2008).

[22] C. Y. Hu, W. J. Munro, J. L. O'Brien, and J. G. Rarity, Phys. Rev. B **80**, 205326 (2009).

[23] C. Bonato, F. Haupt, S. S. R. Oemrawsingh, J. Gudat, D. Ding, M. P. van Exter, and D. Bouwmeester, Phys. Rev. Lett. **104**, 160503 (2010).

[24] C. Y. Hu and J. G. Rarity, Phys. Rev. B **83**, 115303 (2011).

[25] S. M. Tan, J. Opt. B **1**, 424 (1999). The original toolbox was modified to include the QD pure dephasing process.

[26] For a review, see R. J. Warburton, Nat. Mater. **12**, 483 (2013).

[27] In the absence of an external magnetic field, the degeneracy of the electron spin levels could be lifted by the nuclear fields due to the electron-nuclear hyperfine interactions. But the induced electron Zeeman splitting is usually smaller than the linewidth of QD emission; therefore this weak nondegeneracy can be neglected in our work. Note that the degeneracy of the hole spin levels is unaffected due to the lack of the hole-nuclear hyperfine interaction. See J. Hansom, C. H. H. Schulte, C. Le Gall, C. Matthiesen, E. Clarke, M. Hugues, J. M. Taylor, and M. Atatüre, Nat. Phys. **10**, 725 (2014); or for a review, see B. Urbaszek, X. Marie, T. Amand, O. Krebs, P. Voisin, P. Maletinsky, A. Högele, and A. Imamoglu, Rev. Mod. Phys. **85**, 79 (2013).

[28] I. Fushman, D. Englund, A. Faraon, N. Stoltz, P. Petroff, and J. Vučković, Science **320**, 769 (2008).

[29] K. Kheng, R. T. Cox, M. Y. d'Aubigné, F. Bassani, K. Saminadayar, and S. Tatarenko, Phys. Rev. Lett. **71**, 1752 (1993); C. Y. Hu, W. Ossau, D. R. Yakovlev, G. Landwehr, T. Wojtowicz, G. Karczewski, and J. Kossut, Phys. Rev. B **58**, R1766 (1998).

[30] D. F. Walls and G. J. Milburn, *Quantum Optics* (Springer-Verlag, Berlin, 1994).

[31] H. J. Kimble, *Cavity Quantum Electrodynamics*, edited by P. Berman (Academic Press, San Diego, 1994).

[32] C. W. Gardiner and M. J. Collett, Phys. Rev. A **31**, 3761 (1985).

[33] The QD-cavity coupling strength is given by $g = \sqrt{e^2 f/(4\epsilon_r \epsilon_0 m_0 V_{\text{eff}})}$ where f is the X^- oscillator strength, and V_{eff} is the cavity mode volume.

[34] The total QD dipole decay rate defined as $\gamma/2$ in our work is equivalent to $\gamma_\perp$ defined in some other literatures; i.e., $\gamma/2 = \gamma_\parallel/2 + \gamma^* = \gamma_\perp$.

[35] L. Allen and J. H. Eberly, *Optical Resonance and Two-level Atoms* (Dover Publications, New York, 1987).

[36] M. A. Armen and H. Mabuchi, Phys. Rev. A **73**, 063801 (2006).

[37] The saturation nonlinearity starts when the average cavity photon number $\langle n \rangle$ becomes larger than the critical photon number n_c. However, $\langle n \rangle$ is dependent on the input power, the frequency ω, and the coupling strength g; therefore for convenience we use the power P_{in} that is normalized by photons per cavity lifetime to describe the threshold of saturation nonlinearities in our work. It is a complicated function between $\langle n \rangle$ and P_{in} as described by Eqs. (4) and (10).

[38] In the strong-coupling regime, $\langle \sigma_z \rangle$ and $\langle n \rangle$ can have three solutions at some frequencies at intermediate powers. However, we take only one of them in this work. Whether the triple stable phenomenon is real or just caused by the semiclassical approximation is still under investigation.

[39] J. P. Reithmaier, G. Sęk, A. Löffler, C. Hofmann, S. Kuhn, S. Reitzenstein, L. V. Keldysh, V. D. Kulakovskii, T. L. Reinecke, and A. Forchel, Nature (London) **432**, 197 (2004).

[40] T. Yoshie, A. Scherer, J. Hendrickson, G. Khitrova, H. M. Gibbs, G. Rupper, C. Ell, O. B. Shchekin, and D. G. Deppe, Nature (London) **432**, 200 (2004).

[41] E. Peter, P. Senellart, D. Martrou, A. Lemaître, J. Hours, J. M. Gérard, and J. Bloch, Phys. Rev. Lett. **95**, 067401 (2005).

[42] S. Reitzenstein, C. Hofmann, A. Gorbunov, M. Strauß, S. H. Kwon, C. Schneider, A. Löffler, S. Höfling, M. Kamp, and A. Forchel, Appl. Phys. Lett. **90**, 251109 (2007).

[43] T. Volz, A. Reinhard, M. Winger, A. Badolato, K. J. Hennessy, E. L. Hu, and A. Imamoglu, Nat. Photonics **6**, 605 (2012). Here $g/(\kappa + \kappa_s) = 2.7$ was reported for a single InGaAs QD in a photonic crystal nanocavity.

[44] In the low-power regime (i.e., the weak-excitation limit), the first manifold of dressed states are also called normal modes or polariton states, and the corresponding vacuum Rabi splitting is also called the normal mode splitting. Although these concepts can be explained quantum mechanically, the latter can also be explained classically by a coupled oscillator model or linear dispersion theory [see Y. Zhu, D. J. Gauthier, S. E. Morin, Q. Wu, H. J. Carmichael, and T. W. Mossberg, Phys. Rev. Lett. **64**, 2499 (1990)]. However, for simplicity we use the terms of dressed states and Rabi splitting in this work to analyze the results except in some cases specified.

[45] The power dependence of the reflection or transmission spectra can be utilized as an optical detector to measure the efficiency of input light coupling to the QD-cavity systems in experiments.

[46] V. Loo, C. Arnold, O. Gazzano, A. Lemaître, I. Sagnes, O. Krebs, P. Voisin, P. Senellart, and L. Lanco, Phys. Rev. Lett. **109**, 166806 (2012).

[47] D. Englund, A. Majumdar, M. Bajcsy, A. Faraon, P. Petroff, and J. Vučković, Phys. Rev. Lett. **108**, 093604 (2012).

[48] R. Bose, D. Sridharan, H. Kim, G. S. Solomon, and E. Waks, Phys. Rev. Lett. **108**, 227402 (2012).

[49] From Eqs. (3), (4), and (10), we can estimate that the nonsaturation window is closed roughly at $P_{\text{in}} = g^2\gamma_{\parallel}/8\kappa\gamma(\kappa + \kappa_s)$ for single-sided cavity structures, or at $P_{\text{in}} = g^2\gamma_{\parallel}/8\kappa\gamma(2\kappa + \kappa_s)$ for double-sided cavity structures. The higher the coupling strength g, the higher powers the linear GFR and GCB can retain to.

[50] R. Loudon, *The Quantum Theory of Light* (Oxford Scientific Publications, Oxford, 2003).

[51] J. T. Shen and S. Fan, Opt. Lett. **30**, 2001 (2005); S. Fan, S. E. Kocabas, and J.-T. Shen, Phys. Rev. A **82**, 063821 (2010).

[52] E. Waks and J. Vučković, Phys. Rev. Lett. **96**, 153601 (2006).

[53] A. Auffeves-Garnier, C. Simon, J. M. Gerard, and J. P. Poizat, Phys. Rev. A **75**, 053823 (2007).

[54] A. Majumdar, M. Bajcsy, D. Englund, and J. Vučković, IEEE J. Sel. Top. Quantum Electron. **18**, 1812 (2012).

[55] E. T. Jaynes and F. W. Cummings, Proc. IEEE **51**, 89 (1963).

[56] C. Y. Hu *et al.* (unpublished).